Journal of Integrative Neuroscience

J. Integr. Neurosci. **2023**; 22(6): 168
https://doi.org/10.31083/j.jin2206168

Original Research

PKM2 Nuclear Translocation Promotes Glial Cell Activation and Aggravates the Brain Injury of Intracerebral Hemorrhage

Xiao-Yi Xiong[1,2,3,*], Yan-Jing Liang[1], Xin-Xiao Zhang[1], Su-Hao Yang[1], Zhan-Qiong Zhong[4], Shu-Qing Liu[1], Jia-Yi Sun[5], Yong Tang[2,3,6,7], Shu-Guang Yu[1,2,3,*]

[1]Acupuncture and Tuina School, Chengdu University of Traditional Chinese Medicine; 611137 Chengdu, Sichuan, China
[2]Sichuan Provincial Key Laboratory for Acupuncture & Chronobiology, 611137 Chengdu, Sichuan, China
[3]Key Laboratory of Acupuncture for Senile Disease (Chengdu University of TCM), Ministry of Education, 611137 Chengdu, Sichuan, China
[4]School of Basic Medical Sciences, Chengdu University of Traditional Chinese Medicine, 611137 Chengdu, Sichuan, China
[5]Innovative Institute of Chinese Medicine and Pharmacy, Chengdu University of Traditional Chinese Medicine, 611137 Chengdu, Sichuan, China
[6]International Collaborative Centre on Big Science Plan for Purinergic Signalling, Chengdu University of Traditional Chinese Medicine, 611137 Chengdu, Sichuan, China
[7]School of Health and Rehabilitation, Chengdu University of Traditional Chinese Medicine, 611137 Chengdu, Sichuan, China
*Correspondence: xiongxy_89@163.com; xiongxy1989@cdutcm.edu.cn (Xiao-Yi Xiong); ysg28588@126.com; ysg@cdutcm.edu.cn (Shu-Guang Yu)
Academic Editor: Hahn Young Kim
Submitted: 1 August 2023 Revised: 7 September 2023 Accepted: 14 September 2023 Published: 23 November 2023

Abstract

Background: The purpose of this study was to investigate the potential involvement of pyruvate kinase M2 (PKM2), an enzyme acting as a rate-limiting enzyme in the final phase of glycolysis, in the regulation of glial activation and brain damage of intracerebral hemorrhage (ICH). **Methods**: Western blotting and immunofluorescence were performed to investigate PKM2 expression, terminal deoxynucleotidyl transferase deoxyurinary triphosphate (dUTP) nick end labeling staining, hematoxylin and eosin staining, and behavioral tests were employed to evaluate the brain damage of ICH mice, and RNA-seq and bioinformatic analyses were performed to detect gene expression changes in ICH mice treated with TEPP-46. **Results**: Increased PKM2 levels in perihematomal brain tissue were found starting from 3 days following ICH and peaked at 5 and 7 days post ICH. The increased expression of PKM2 was mainly co-localized with glial fibrillary acidic protein $(GFAP)^+$ astrocytes and ionized calcium binding adaptor molecule-1 $(IBA\text{-}1)^+$ microglia. Furthermore, we observed a notable increase in the nuclear translocation of PKM2 in glial cells following ICH. TEPP-46 treatment significantly reduced PKM2 nuclear translocation, and effectively attenuated glial activation and brain injury, and improved functional recovery of mice with ICH. RNA-seq data indicated that 91.1% (205/225) of differentially expressed genes (DEGs) were down-regulated in the TEPP-46 treated groups compared with the vehicle-treated groups in ICH brains. Furthermore, bioinformatic analyses revealed that these down-regulated DEGs were involved in a variety of biological processes, including autophagy and metabolic processes. In addition, the majority of these downregulated DEGs had a primary high expression in neurons, with subsequent expression seen in endothelial cells, microglia, and astrocytes. **Conclusions**: These results indicate that increased PKM2 nuclear translocation promotes the activation of glial cells after ICH, hence aggravating ICH-induced brain damage, and aggravates the brain injury induced by ICH. This highlights a potential therapeutic target for inhibiting glial activation to attenuate brain injury after ICH.

Keywords: PKM2; glial cell; brain injury; intracerebral hemorrhage

1. Introduction

Intracerebral hemorrhage (ICH) is a leading cause of morbidity and mortality worldwide [1], with fatality rates ranging from 40–54% at 1 month to 1 year after the index event [2]. Even though current stroke guidelines recommend early, positive, goal-directed treatment for ICH patients [1], there are currently no effective neuroprotective strategies for reducing brain injury in ICH patients, due to the risk of early neurological impairment and worse clinical outcomes.

Neuroinflammation has been identified as one of the key contributors to the aggravation of brain damage after ICH [3,4]. Furthermore, neuroinflammation is emerging as an instigator rather than an outcome in the pathogenic process of numerous brain diseases [5]. Glial cells (e.g., astrocytes and microglia) have been identified as the primary inflammatory cells in several neurological disorders, including stroke. Consequently, inhibiting glial activation may be a promising strategy for reducing the neuroinflammation-mediated brain injury caused by ICH [4]. Energy is an essential component for supporting cellular life and biofunctions, particularly for cells that transition from a resting to an active state. Accordingly, glial cell activation is mostly reliant on energy support. Mounting evidence indicates that glial cells mainly consume the energy produced by glycolysis to promote their activation [6–8]. Pyruvate kinase M2 (PKM2) is a rate-limiting, glycolytic enzyme that orchestrates the final step in the glycolytic pathway by catalyzing the conversion of phosphoenolpyruvate (PEP) and adeno-

sine diphosphate (ADP) to pyruvate and adenosine triphosphate (ATP) [9,10]. PKM2 is expressed in a wide range of proliferating cells, including embryonic cells, adult stem cells, tumor cells, and immune cells [11–14]. Their elevated rates of nucleic acid synthesis are a shared characteristic. It is noteworthy that PKM2 has dual functionality, serving not only as a metabolic enzyme but also as a protein kinase and transcriptional coactivator [10]. The enzymatic activity of PKM2 is closely related to oligomerization states, that is tetramer form for active, dimer form for less active, and monomer form for inactive [15–18]. As a direct consequence of detetramerization, PKM2 monomer translocases to the nuclear and acts as a protein kinase/transcriptional coactivator to regulate gene transcription [18–20]. However, the role of PKM2 as a protein kinase in regulating brain injury in central nervous system (CNS) diseases, particularly ICH, are poorly understood.

Therefore, we examined the kinase activity of PKM2 in regulating glial activation and brain damage following ICH in this investigation. We showed that the up-regulated expression of PKM2 and increased nuclear translocation of PKM2 in the perihematomal brain tissues coincided with glial activation following ICH. While TEPP-46, a PKM2 tetramer stabilizing activator, significantly inhibited PKM2 translocation, leading to a reduction in glial activation and subsequent brain injury following ICH. Subsequently, RNA-seq technology was employed to investigate potential mechanisms. The results revealed that about 90% of differentially expressed genes (DEGs) were downregulated in response to TEPP-46 treatment in mice with ICH. These DEGs are likely to have important roles in the modulation of autophagy, metabolic processes in neurons, endothelial cells, microglia, and astrocytes. The present work offers a unique perspective on the protein kinase functions of PKM2 in the regulation of ICH-induced brain damage, as well as prospective therapeutic targets for ICH therapy.

2. Materials and Methods

2.1 Mice

This study used C57BL/6 mice (male, 8 weeks, 23 $\pm$ 2 g) purchased from Gempharmatech (Chengdu, China). Mice were housed in a pathogen-free environment with a 12-hour/12-hour light/dark cycle, 25 °C ambient temperature, and 45–55% relative humidity. They had unrestricted access to food and water. The Animal Experimentation Ethics Committee of Chengdu University of Traditional Chinese Medicine (Chengdu, China) granted approval for all animal experiments in accordance with established procedures. All experiments were conducted in accordance with the National Academy of Sciences and National Institutes of Health's Guide for the Care and Use of Laboratory Animals. No abuse or maltreatment occurred during our study.

2.2 Construction of the Intracerebral Hemorrhage Mouse Model

We constructed the ICH mouse models according to our previously developed methods [21,22]. Briefly, a stereotaxic apparatus (RWD Life Science Co., Shenzhen, Guangdong, China) was applied to immobilize mice after they were anesthetized with 3% and 1.5% isoflurane (Cat# R510-22-10, RWD Life Science Co., Shenzhen, China), respectively, for anesthesia induction and maintenance. A total volume of 0.5 µL type VII collagenase (0.075 IU, C0773, Sigma Aldrich, St. Louis, MO, USA) was continuously injected into the mouse left striatum (0.8 mm anterior, 2 mm lateral to bregma, and at a depth of 3.5 mm) using a syringe pump (Legato 130, RWD Life Science Co., Shenzhen, China). Control mice received saline injection (0.5 µL). Mouse body temperature was maintained at 37 °C throughout surgery and anesthesia resuscitation. After recovery from anesthesia, a Longa score $\geq$1 indicated the success of ICH model construction. The death rate and success rate of ICH mice was 3.41% and 92.04%, respectively. We discarded all ICH model mice that were deemed unsuccessful, either due to being asymptomatic or that resulted in death. TEPP-46 (HY-18657, MedChemExpress, Middlesex County, NJ, USA) at a dosage of 50 mg/kg was intraperitoneally injected into ICH mice once a day for 5 consecutive days, starting 6 hours after ICH.

2.3 Western Blotting

According to our previously reported method [23], western blots were performed for assessing the PKM2 levels in the perihematomal brain tissues of ICH mice. Briefly, the ipsilateral brain tissues and control brain tissues of mice were collected and homogenized to extract proteins using a prepared radio immunoprecipitation assay (RIPA) lysis buffer (Beyotime, Shanghai, China), and a Bicinchoninic Acid (BCA) protein assay (Cat# 23227/23225, Thermo Scientific, Waltham, MA, USA) was used to determine the protein concentration. Proteins were resolved by sodium dodecyl sulphate-polyacrylamide gel electrophoresis (SDS-PAGE) and electroblotted onto polyvinylidene fluoride (PVDF; Millipore, Burlington, MA, USA) membranes after adjustment to the same final concentration. Next, after blocking the membranes for 2 hours at room temperature with 5% non-fat milk in tris-buffered saline containing 0.1% Tween-20 (TBST; Biosharp, Guangzhou, Guangdong, China), they were incubated with anti-PKM2 (#4053, 1:50, Cell Signaling Technology, Danvers, MA, USA) antibody overnight at 4 °C. The membranes were then washed four times with TBST and incubated with a secondary antibody conjugated with horseradish peroxidase (HRP) (1:2500; OR03L, Sigma-Aldrich, St. Louis, MO, USA) at room temperature for 2 hours. An enhanced chemiluminescent (ECL) substrate was used to view the immunoreactive proteins with an imaging system (GelView 6000Plus, Guangzhou Biolight Biotechnology Co., Ltd.,

Guangzhou, Guangdong, China). Following stripping, the membranes were incubated again with glyceraldehyde-3-phosphate dehydrogenase (GAPDH; Cat# 60004-1-Ig, Proteintech, Wuhan, Hubei, China) acting as the loading control. The band intensities were normalized to the values for GAPDH and quantified using Image J software (version 1.46J, National Institutes of Health, Bethesda, MD, USA).

2.4 Immunofluorescent Staining and Analysis

Based on our previously reported procedures [23], we performed immunohistochemical staining to investigate the PKM2 expression profiles in the brains of ICH mice. The mice were sedated and their brains were rapidly removed and preserved in 4% paraformaldehyde (PFA; Cat# P1110, Solarbio, Beijing, China) at 4 °C overnight, after being intracardially perfused with PBS and 4% paraformaldehyde. Brain sections of 15 µm were then incubated with the following antibodies: anti-PKM2 (#4053, 1:50, Cell Signaling Technology, USA), Iba-1 (ab178846, 1:200, Abcam, Cambridge, MA, USA), NeuN (#24307, 1:200, Cell Signaling Technology, USA), and glial fibrillary acidic protein (GFAP; ab7260, 1:300, Abcam, USA). Secondary antibodies, including Alexa Fluor 594 (1:200, donkey anti-rabbit), Alexa Fluor TRITC (1:200, rabbit anti-goat), and Alexa Fluor 488 (1:200, donkey anti-mouse), were purchased from Proteintech Group (Wuhan, Hubei, China). The brain slices were imaged using confocal microscopy (Olympus IXplore SpinSR10, Olympus, Tokyo, Japan). Quantification of double-labeled cells was used to calculate the ratio of co-labeled cells. Three brain slices were selected from each mouse brain at random; double-labeled cells were counted automatically, and the average data obtained by three independent researchers who were unaware of group information was used to determine the value for each brain.

2.5 Hematoxylin and Eosin (H&E) Staining

After the mice were euthanized, their brains were rapidly removed and fixed in a 10% neutral-buffered formalin solution (Cat# G2161, Solarbio, Beijing, China). Following dehydration in ethanol solutions, the brain tissues were embedded in paraffin. The brain tissues were then sectioned at 5 µm thickness using a rotary microtome. Lastly, three slices of each brain tissue were selected at random, then stained with H&E, and viewed under an Olympus microscope (Olympus SLIDEVIEW VS200, Olympus, Tokyo, Japan) to evaluate the damage in these perihematomal brain tissues.

2.6 Terminal Deoxynucleotidyl Transferase Deoxyurinary Triphosphate (dUTP) Nick End Labeling (TUNEL) Staining

Based on the manufacturer's instructions of a commercial One-step TUNEL In Situ Apoptosis Kit (E-CK-A320, Elabscience, Wuhan, Hubei, China), TUNEL staining was performed. Briefly, 10 µL 1 × protease K working solution was added to the three slices of each mouse brain selected randomly and incubated at 37 °C for 10 min. The brain slices were then washed three times with PBS for 5 min each. The sections were then incubated with 100 µL 1 × DNase I Buffer at room temperature for 5 min. After removing excess liquid from the sample, 100 µL diluted DNase I working solution (200 U/mL) was added to each brain section, then incubated at 37 °C for 10–30 min. After washing with PBS, 100 µL TdT Equilibration Buffer was added to each brain slice and incubated at 37 °C for 10~30 min. After removing the TdT Equilibration Buffer, 50 µL marker working solution was added and incubated at 37 °C for 60 min in a wet box in the dark. Finally, 4,6-diamino-2-phenyl indole (DAPI; Cat# G1012-100ML, Servicebio, Wuhan, Hubei, China) solution was added to stain the nucleus. The TUNEL-stained brain slices were observed under a Lycra microscope (Leica DM6B, Leica AG, Wetzlar, Germany). For further analysis of the TUNEL results, three researchers who were unaware of the group information independently evaluated the number of positive cells in each standardized microscopic field in the perihematomal brain tissues using ImageJ software (version 1.46J, National Institutes of Health, USA).

2.7 Behavioral Test

The corner test was conducted using previously published procedures [24,25]. ICH mice were first placed between two cardboard pieces with a 30° angle corner. The operator progressively moved the board toward the mouse while preserving a 30° angle, until the mouse was near the corner, at which point the board was lifted and rotated 180° to face the open end. Each mouse was evaluated 10 times, and the direction in which it turned during each trial (left or right) was recorded. Behavioral testing was performed on 10 independent mice in each group, and the number of right (R) and left (L) turns was recorded. This was used to calculate an overall score = [(R)/(R+L)] × 100%. Subsequently, the mouse was placed in a fresh cage in order to evaluate its sensory neglect using the adhesive tape removal task. The adhesive tape was affixed to the planter area of the left and right front paws of the mouse, and the time it took for each paw to successfully remove the tape was recorded. Up to 300 seconds of testing was permitted for each paw.

2.8 RNA-seq

Perihematomal brain tissue of ICH mice, after treatment with or without TEPP-46 at 5 days post ICH, was collected for sequencing. Brain tissue total RNA was extracted, and cDNA libraries were constructed using an Oxford Nanopore Technologies (ONT)-supplied Ligation Sequencing Kit 1D (PM) (SQK-LSK110, Oxford Nanopore Technology, Oxford, England) in accordance with the company's protocol. Full-length cDNA was enriched using reverse transcriptase and the addition of defined PCR adapters to both ends of the first strand of cDNA, then 14-circle

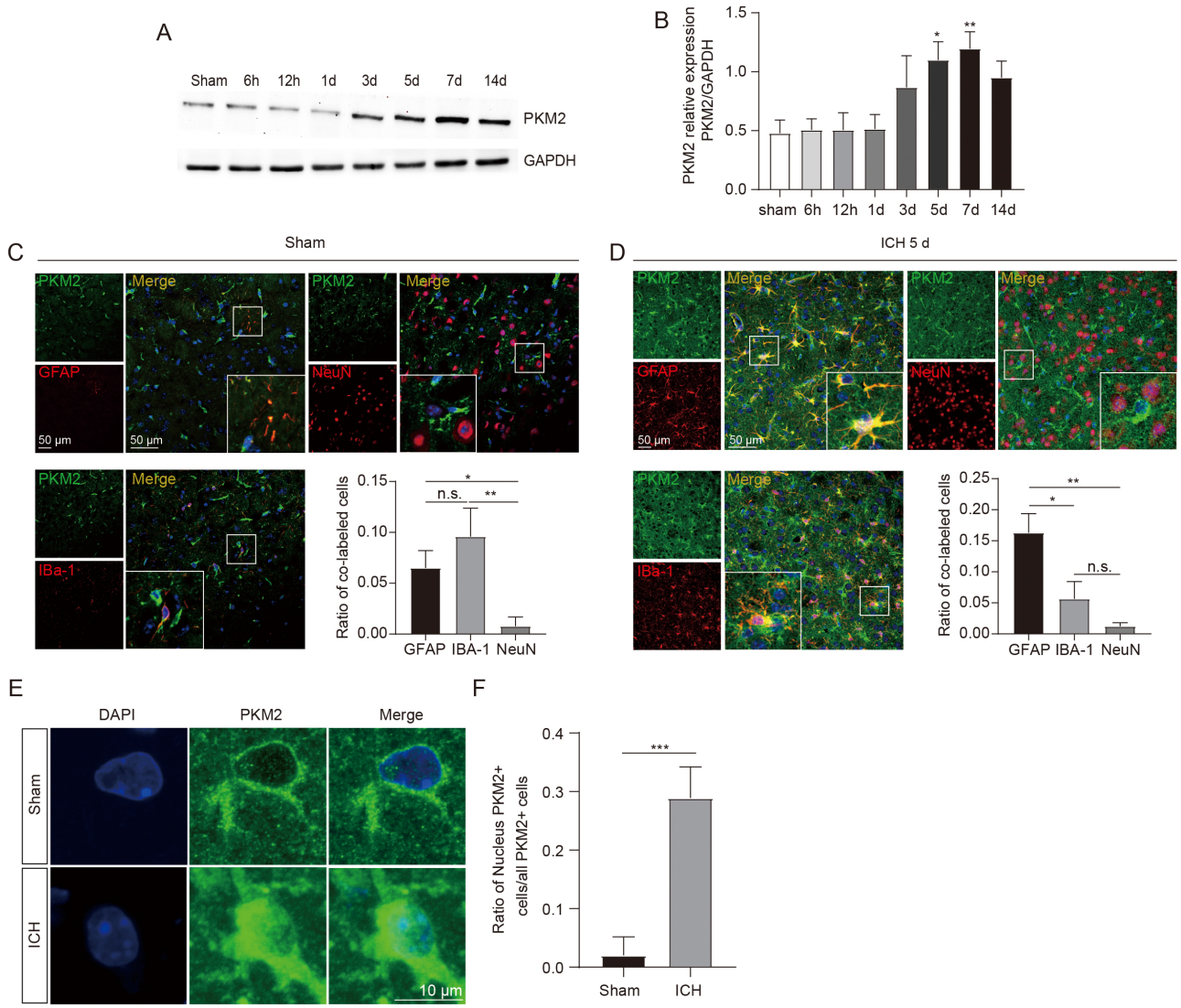

Fig. 1. PKM2 expression profiles in the perihematomal brain tissues of ICH mice. (A,B) Representative image of western blot (A) and statistical analysis (B) of PKM2 expression in the perihematomal brain tissues at different time points after ICH (each time point, n = 5 for each group). (C,D) Immunofluorescent staining of cells expressing PKM2 with NeuN+ neurons, IBA-1+ microglia, and GFAP+ astrocytes in sham (C) and ICH mice (D), respectively (n = 4 for each group). (E) Representative immunofluorescent image of PKM2 nuclear translocation in the perihematomal brain tissues at 5 days following ICH. (F) Statistical results of immunofluorescent staining. n = 4 for each group. *$p < 0.05$, **$p < 0.01$, and ***$p < 0.001$ vs sham controls; n.s. indicates not statistically significant. PKM2, pyruvate kinase M2; ICH, intracerebral hemorrhage; IBA-1, ionized calcium binding adaptor molecule-1; GFAP, glial fibrillary acidic protein; GAPDH, glyceraldehyde-3-phosphate dehydrogenase; DAPI, 4,6-diamino-2-phenyl indole.

cDNA PCR (8 min extension time) was performed using LongAmp Tag DNA polymerase (New England Biolabs, Ipswich, MA, USA). T4 DNA ligase (New England Biolabs, Ipswich, MA, USA) was then used to bind the PCR products to the ONT adaptor ligation. DNA purification was performed using Agencourt XP beads (Beckman Coulter, Brea, CA, USA). A PromethION platform of the Biomarker Technology Company (Beijing, China) was used to analyze the final cDNA libraries after being processed by FLO-MIN109 flow cells (FLO-PRO002, Oxford Nanopore Technology, Oxford, England).

2.9 Bioinformatic Analysis

Raw reads with an average quality score of less than 7 and a length of less than 500 bp were eliminated. After the rRNA was mapped to the rRNA database, it was discarded. Next, primers at both ends of the reads were searched to identify the full-length, non-chimeric (FLNC) transcripts. The Mimimap2 alignment program [26] was applied to the reference genome library in order to obtain clusters of FLNC transcripts. Full-length reads were mapped to the reference genome (Rnor_5.0). Reads with match quality more than 5 were further used for quanti-

tative analysis. Counts per million (CPM) [27] was used as an indicator to measure the levels of transcript or gene expression. Using the DESeq R package (DESeq2 1.6.3, Germany; http://www.bioconductor.org/packages/release/bioc/html/DESeq2.html), DEGs between the two groups were analyzed. The *p*-values were adjusted using Benjamini and Hochberg's approach, and the DEGs induced by TEPP-46 treatment were defined as those with a *p*-value < 0.05 and a fold change (FC) ≥ 1.5. The subcellular location information of the proteins encoded by down-regulated DEGs induced by TEPP-46 was collected from the UniProt database (http://www.uniprot.org/database/) [28]. The Goseq R package based on Wallenius noncentral hypergeometric distribution was used for Gene Ontology (GO) enrichment analysis of the down-regulated DEGs, which can adjust for the bias in gene length of DEGs. Kyoto Encyclopedia of Genes and Genomes (KEGG) analysis was performed to analyze the statistical enrichment of down-regulated DEGs using KOBAS software (http://kobas.cbi.pku.edu.cn/index.php).

2.10 Integrative Analysis of the Down-Regulated DEGs Induced by TEPP-46 and Transcriptome Data

Conjoint analysis was performed using our published method [21,22] by matching the down-regulated DEGs induced by TEPP-46 with previously published transcriptome data [29]. Considering the extensive research conducted on brain cells in the context of stroke, including neurons, glial cells (e.g., astrocytes and microglia), and endothelial cells, these four cell types were selected for further analysis. Firstly, the relatively high expression of genes in the four cells were defined using previous methods [21,22]. For example, gene A is defined as being highly specific to astrocytes when the ratio of the fragments Per Kilobase of exon model per Million fragments mapped (FPKM) of gene A in astrocytes to that in the other three neural cells (neurons, microglia, and endothelial cells) is >10.0 and being highly expressed in neurons is defined as having a ratio >1.0. To further identify close relationships between down-regulated DEGs and neurons, glial cells, and endothelial cells, an association matching analysis was performed by matching the down-regulated DEGs with the highly expressed genes in each type of neural cell.

2.11 Statistical Analysis

The data were presented as the mean $\pm$ standard deviation (SD), and were analyzed using SPSS 26.0 statistical software (IBM Corp., Armonk, NY, USA). For pairwise comparisons, nonparametric Wilcoxon-Mann-Whitney tests were conducted, while the nonparametric Kruskal-Wallis test was applied for comparisons among more than two groups. Values of $p < 0.05$ were considered statistically significant.

3. Results

3.1 Upregulated Expression of Glial PKM2 in Perihematomal Brain after ICH

To determine the role of PKM2 in ICH-induced brain damage, we analyzed the expression profiles of PKM2 in the perihematomal brain tissues following ICH. First, we performed a western blot and observed that PKM2 levels were significantly elevated beginning 3 days after ICH, peaked at 5 and 7 days, and remained elevated at day 14 compared with sham groups (Fig. 1A,B). The expression levels of PKM2 and the cellular sources of PKM2 in ICH mouse brains were further analyzed by the immunofluorescent staining. In the sham groups, the total PKM2 expression level was low, and PKM2 expression was mostly localized in glial cells, particularly in the IBA-1-positive microglia, even though these cells were not activated (Fig. 1C). In contrast, in the perihematomal brain tissues of mice at 5 days after ICH, we found that PKM2 expression and glial activation were both significantly increased, and PKM2 was mainly co-localized with GFAP-positive astrocytes, followed by IBA-1 positive microglia, and rarely co-localized with NeuN-positive neurons (Fig. 1D). These data revealed a dynamic change feature of PKM2 expression after ICH, in which low and microglial PKM2 expression gradually switches to high and astrocytic expression in response to the brain damage caused by ICH.

3.2 Increased PKM2 Nuclear Translocation in Glial Cells after ICH

The enzymatic activity of PKM2 is closely related to its oligomerization status, including active tetramer, less active dimer, and inactive monomer [18]. PKM2 detetramerization directly leads to the nuclear translocation of its inactive monomer [20], which has been shown to regulate gene transcription by functioning as a protein kinase in the nucleus. [18,19,30]. Our immunofluorescent staining data was analyzed to determine the PKM2 oligomerization status after ICH by evaluating the nuclear expression levels. In the sham groups, low PKM2 expression was observed mostly in the cytoplasm, whereas 30% of PKM2-positive cells exhibited nuclear translocation in the ICH mice (Fig. 1E,F), suggesting an ICH-induced shift to PKM2 monomers. TEPP-46, a small-molecule activator that stabilizes PKM2 in its tetramer form [31], was then intraperitoneally injected into ICH mice for 5 consecutive days. The results demonstrated that TEPP-46 treatment notably prevented the nuclear translocation of PKM2 in the perihematomal brain tissues of ICH mice, compared with ICH mice treated with a vehicle (Fig. 2A,B). This indicates that increased PKM2 nuclear translocation in glial cells resulting from the PKM2 detetramerization induced by ICH may participate in the regulation of glial cell activation and brain injury, as PKM2 nuclear translocation has been shown to promote the activation of immune cells [13].

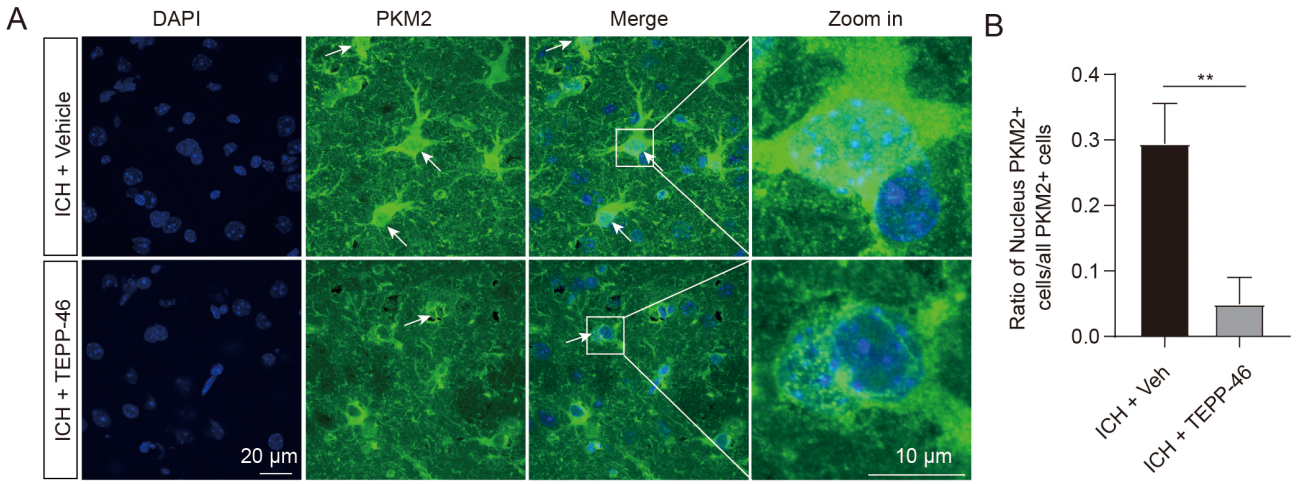

Fig. 2. TEPP-46 treatment markedly reduced the PKM2 nuclear translocation after ICH. (A) Representative immunofluorescent image showing that TEPP-46 induced a significant reduction of PKM2 nuclear translocation in the perihematomal brain tissues at 5 days after ICH. (B) Statistical results of immunofluorescent staining. n = 4 for each group, $^{**}p < 0.01$ vs sham controls.

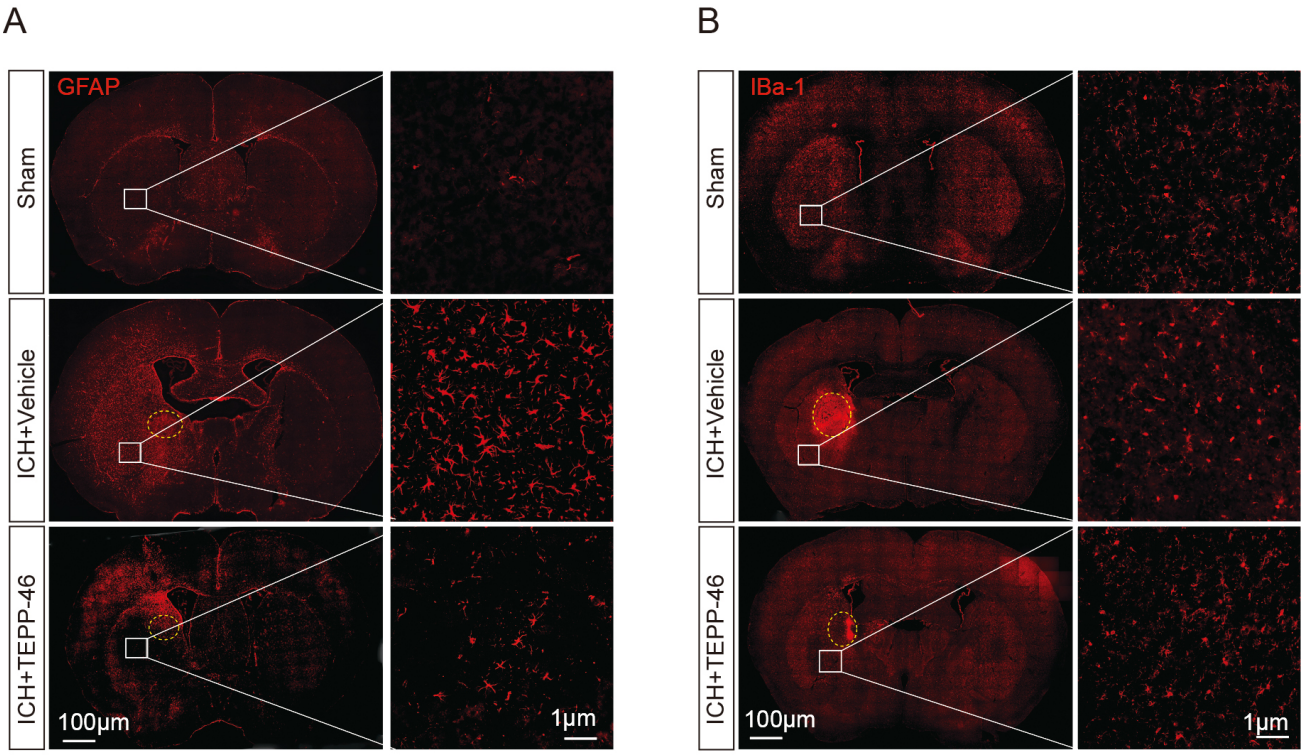

Fig. 3. Glial activation was significantly inhibited after ICH treated by TEPP-46. The activation of $GFAP^+$ astrocytes (A) and $IBA\text{-}1^+$ microglia (B) were inhibited in ICH mice at 5 days after TEPP-46 treatment (n = 4 for each group).

3.3. TEPP-46 Treatment Reduced the Activation of Glial Cells, Attenuated Brain Injury, and Improved Functional Recovery of Mice with ICH

Through the evaluation of glial markers, it was shown that the mice in the vehicle-treated ICH group had a significant increase in the presence of activated astrocytes (Fig. 3A) and microglia (Fig. 3B) inside the perihematomal brain tissue, as compared with the sham group. In contrast, the TEPP-46 treatment significantly reduced both the activation of astrocytes and microglia after ICH (Fig. 3), suggesting that PKM2 detetramerization promoted glial activation after ICH. H&E staining was conducted to assess the general brain injury and we observed that TEPP-46 treatment resulted in a reduction of brain injury in the perihematomal brain tissues at 5 days post ICH. (Fig. 4A). Similarly, TEPP-46 treatment reduced the in-

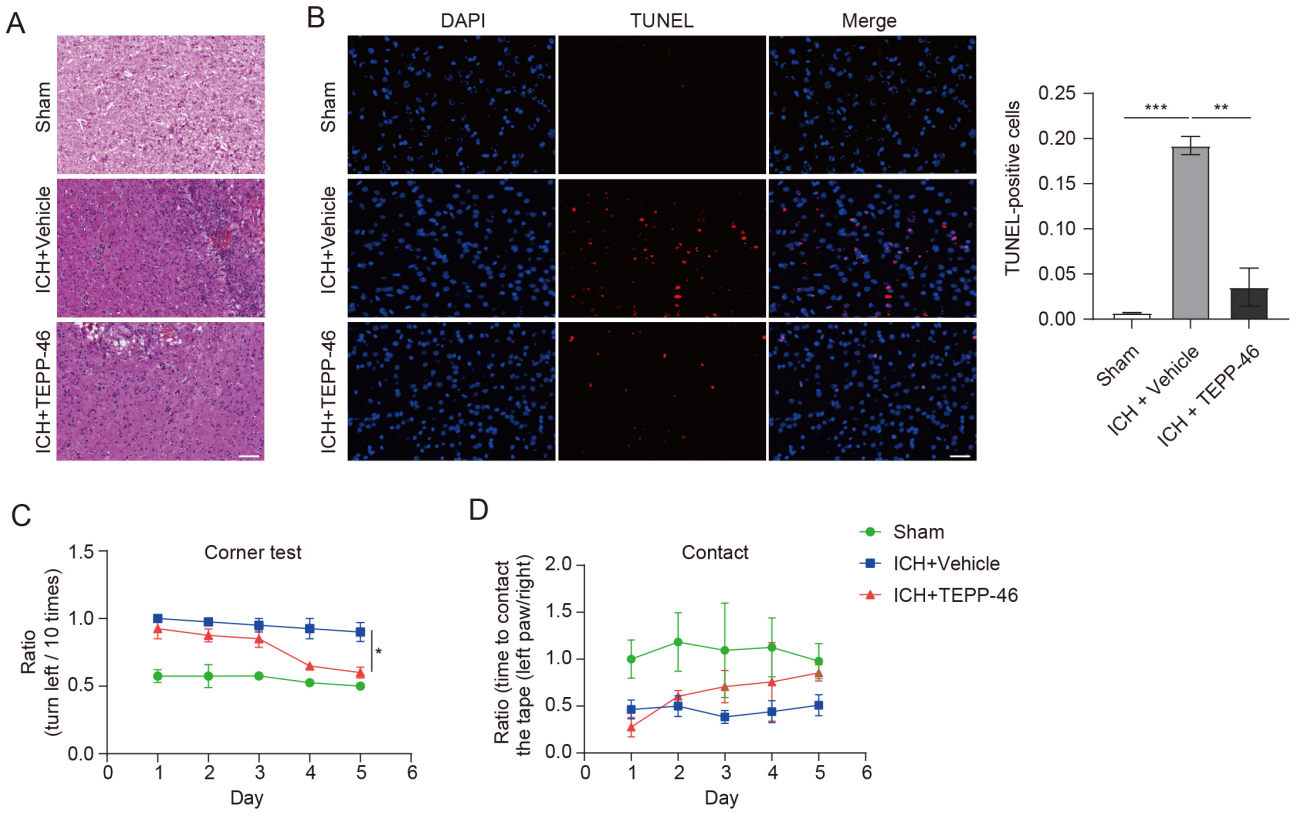

Fig. 4. TEPP-46 treatment markedly reduced brain injury and improved functional recovery of mice with ICH. (A) H&E staining shows that brain injury and infiltration of immune cells were markedly reduced in ICH mice treated with TEPP-46 (n = 4 for each group). (B) TUNEL+ cells were obviously reduced in ICH mice treated with TEPP-46 (n = 4 for each group, $^{**}p < 0.01$, $^{***}p < 0.001$). (C) TEPP-46 treatment markedly enhanced performance on the corner test (a measure of spatial neglect, n = 10 for each group; $^{*}p < 0.05$ vs vehicle-treated ICH mice) at 4 and 5 days post ICH. (D) TEPP-46 treatment did not markedly enhance performance on the tape removal task (a measure of sensory neglect, n = 10 for each group; $p > 0.05$). Scale bar = 100 μm for (A) and = 50 μm for (B). TUNEL, Terminal Deoxynucleotidyl Transferase Deoxyurinary Triphosphate (dUTP) Nick End Labeling.

creased TUNEL+ cells in the brain tissue surrounding the hematoma (Fig. 4B). In the corner tests, the TEPP-46-treated ICH mice almost recovered from their physical disability within 5 days (Fig. 4C), which was consistent with the results of the PKM2 expression profile. However, the sensory neglect of mice with ICH was not significantly improved after TEPP-46 treatment, although there was a trend for improvement (Fig. 4D). These results strongly indicate that TEPP-46 treatment reduces brain injury and partly improves functional recovery of ICH that may be related to the inhibition of glial activation by preventing PKM2 nuclear translocation in glial cells.

3.4 The Neuroprotective Effects of TEPP-46 Treatment May be Related to a Large Number of Down-Regulated DEGs Regulating the Functions of Neural Cells after ICH

RNA-seq was then performed on perihematomal brain tissue from ICH mice treated with or without TEPP-46 to obtain insight into the molecular consequences of glial inhibition induced by PKM2 tetramerization (Fig. 5A). Surprisingly, 91.1% (205/225) of DEGs were down-regulated in the ICH mouse brains treated by TEPP-46 compared with those treated with vehicle (Fig. 5B), indicating that most of the upregulated DEGs induced by ICH may have been inhibited when PKM2 nuclear translocation was blocked. The proteins encoded by these down-regulated DEGs were widely distributed throughout the cells, including in the nucleus and cytoplasm (Fig. 5C). An analysis of these down-regulated DEGs using GO term enrichment analyses revealed that TEPP-46-treated mice, when compared with vehicle controls, had decreased responses to autophagy and its related biological processes, metabolic processes, receptor complex, and membrane-related events (Fig. 5D). In addition, KEGG pathway analysis found that the majority of these downregulated DEGs were enriched in the PI3K-Akt signaling pathway, autophagy, Ras signaling pathway, chemokine signaling pathway, and Wnt signaling pathway (Fig. 5E); all of which have been shown to be closely related to ICH brain damage.

As the assessed samples were perihematomal brain tissues, cellular information regarding changes at the transcriptome levels was lost. To demonstrate that TEPP-46

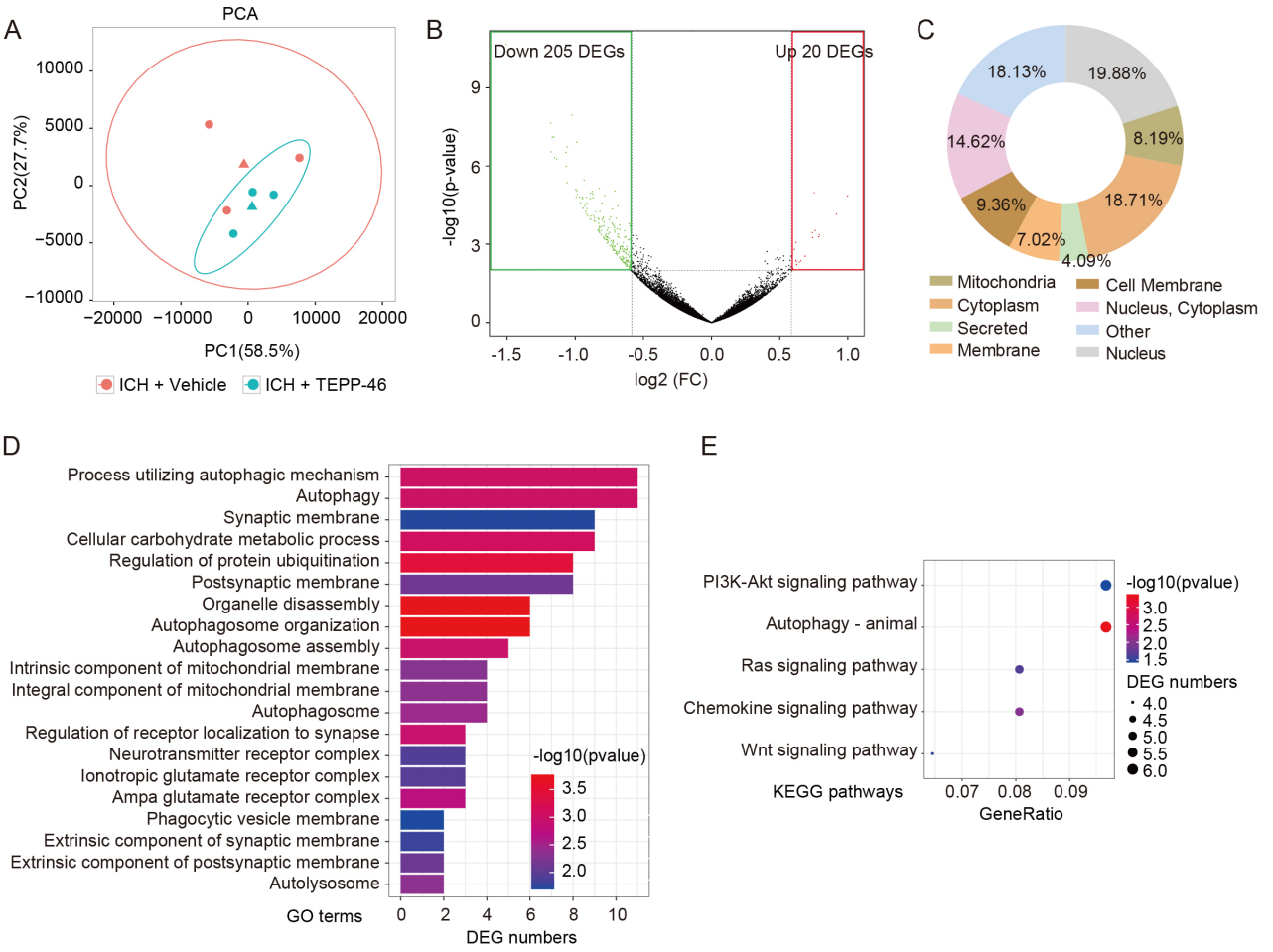

Fig. 5. Analysis of RNA-seq data of ICH brains. (A) PCA analysis reveals the dispersion degree of the transcriptome between the TEPP-46- and vehicle-treated ICH brains. (B) The volcano plot shows the down-regulated and up-regulated DEGs induced by TEPP-46 treatment for ICH brains compared with the vehicle-treated brains. (C) The subcellular localization of proteins encoded by down-regulated DEGs in (B). (D,E) GO (D) and KEGG (E) analysis of the down-regulated DEGs in (B). (n = 3 for each group). PCA, Principal Component Analysis; FC, fold change; DEGs, differentially expressed genes; GO, Gene Ontology; KEGG, Kyoto Encyclopedia of Genes and Genomes.

treatment induced alterations in the transcriptome of neural cells in response to ICH injury [29], we performed a conjoint analysis of previously published RNA-seq data of brain cells and our down-regulated DEGs using our previously published methodologies [21,22]. After comparing the highly expressed genes of brain cells [21,22] with the down-regulated DEGs, we showed that the majority of the DEGs were relatively highly expressed in neurons, microglia, endothelial cells, and astrocytes (Fig. 6A); 37.56% of total down-regulated DEGs were identified in neurons, 17.56% in microglia, 17.07% in endothelial cells, and 13.17% in astrocytes (Fig. 6A). Considering that the levels of mRNA expression in cells vary greatly, and that higher mRNA expression may be important for cell function, the specificity ratio of the DEGs was further analyzed to evaluate whether these down-regulated DEGs induced by TEPP-46 treatment could potentially influence the biofunction of neural cells. The results depicted by pie charts indicate that 12 down-regulated DEGs (*Gng4*, *Larp6*, *Bhlhe22*, *Fam19a2*, *Efna3*, *Npas1*, *Hs6st3*, *Cnksr2*, *Ank1*, *Crmp1*, *Vstm2l*, and *Ccdc92*) with a specificity ratio >10 in neurons (Fig. 6B, upper right). For astrocytes and microglia, there were two DEGs with specificity ratios >10 (*Igfbp2* and *Btbd17* for astrocytes, *Gns* and *Limd2* for microglia; Fig. 6B, left), respectively. Only a single DEG with a specificity ratio >10 was detected in endothelial cells (*Sox17*; Fig. 6B, lower right). Furthermore, the specificity ratios of DEGs in the four brain cell types exhibited a range of 1–3 (Fig. 6B). Notably, endothelial cells and microglia had a very high proportion; more than 72% of the specificity ratios were <2 (Fig. 6B). These findings demonstrate that TEPP-46 treatment may have a direct impact on the functioning of glial cells, as well as an indirect influence on other cellular processes inside the brain, hence providing a neuroprotective effect against ICH.

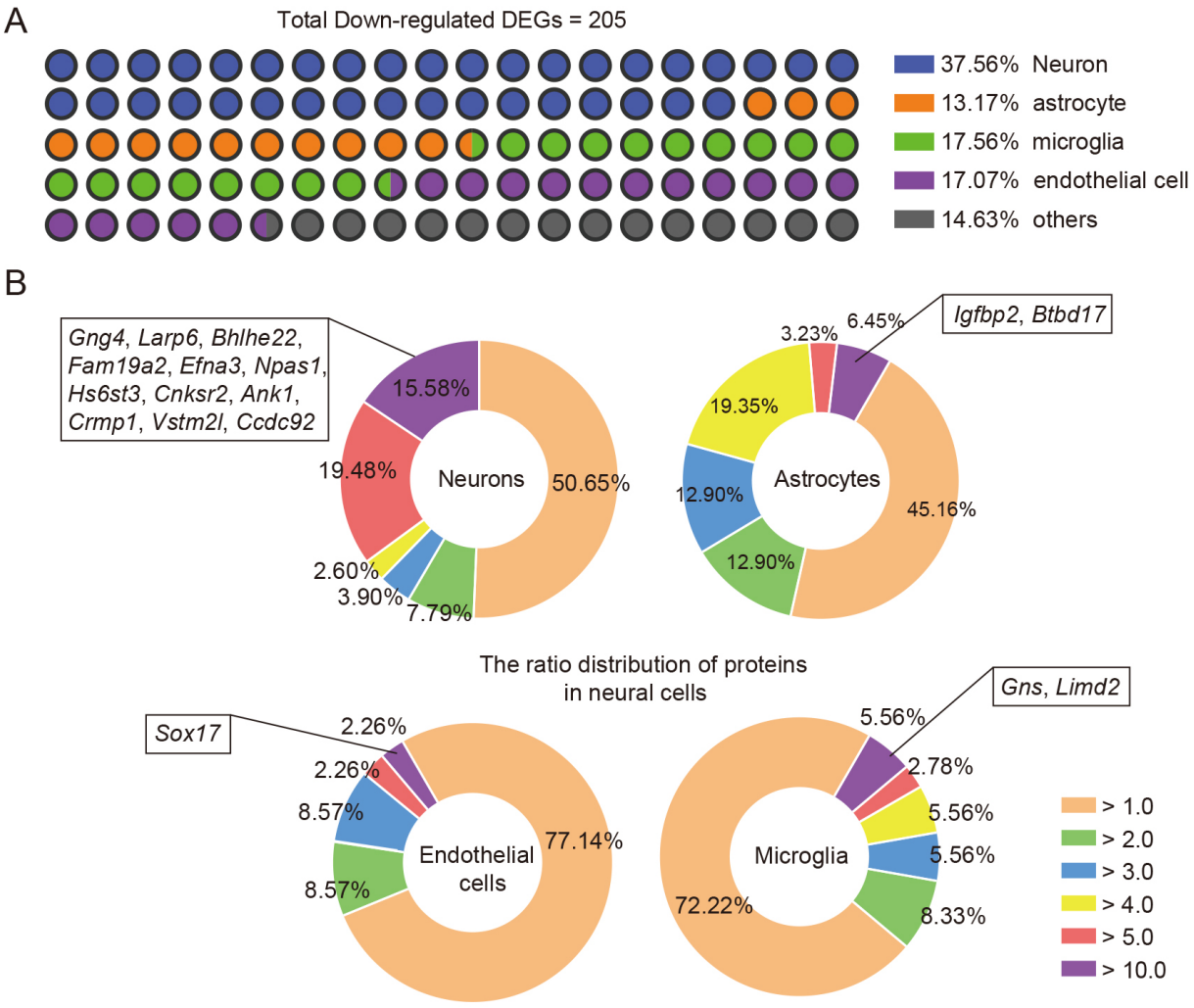

Fig. 6. Combined analysis of the down-regulated DEGs of ICH brains induced by TEPP-46 and transcriptomics data. (A) The major cellular distributions of down-regulated DEGs of ICH brains after TEPP-46 treatment compared with vehicle treatment. (B) The pie charts show the specificity ratio distribution of the down-regulated DEGs in neurons (upper left), astrocytes (upper right), microglia (lower right), and endothelial cells (lower left).

4. Discussion

The switching of the role of PKM2 from metabolic enzyme to protein kinase is tightly related to its oligomerization states, such as tetramer for metabolic activity and monomer for kinase. The latter is a direct result of PKM2 detetramerization, which leads to nuclear translocation to exert its protein kinase activity. We investigated the role and potential mechanism of the protein kinase PKM2 in the regulation of brain injury after ICH. Our results revealed that the PKM2 expression level in perihematomal brain tissues was increased in reactive astrocytes and microglia of ICH mice, and about 30% of the PKM2-positive cells exhibited nuclear translocation. The treatment of ICH mice with TEPP-46, a small-molecule activator stabilizing PKM2 in tetramer form, resulted in decreased glial cell activation, reduced brain injury, and enhanced functional recovery, as well as the inhibition of PKM2 nuclear translocation. Mechanistically, TEPP-46 treatment induced a significant number of down-regulated DEGs, which may be associated with regulating neural cell functions after ICH, according to RNA-seq analysis. Consequently, we presented evidence for the regulation of brain injury and glial activation by PKM2 protein kinase, identifying a unique therapeutic target for inhibiting PKM2 nuclear translocation in order to alleviate brain injury and glial activation after ICH.

PKM2 is highly expressed in cancer cells and activated immune cells, which may be attributable to the fact that PKM2 catalyzes the final and rate-limiting reaction in the glycolytic pathway, as these cells consume much energy to support their biological processes. Interfering with PKM2 prevents cancer cell metabolism and proliferation by inhibiting the aerobic glycolysis of cancer cells [32–34]. Furthermore, the activation of NOD-like receptor thermal protein domain associated protein 3 (NLRP3)

and absent in melanoma 2 (AIM2) inflammasomes [35] as well as the release of high mobility group box 1 (HMGB1) protein [12] are exacerbated by PKM2-mediated glycolysis in macrophages. This exacerbation contributes to the progression of lethal endotoxemia and sepsis, hence enhancing the toxic impact of macrophages. Furthermore, a recent study demonstrated that pharmacological inhibition of PKM2 moderated microglial activation and enhanced spatial learning and memory in Alzheimer's disease mice. This was due to the exacerbation of microglial dysfunction induced by the positive feedback loop involving glycolysis/H4K12la/PKM2 [14]. The aforementioned studies have provided insight into the role and mechanism of PKM2 in disease progression, with particular emphasis on its function as a metabolic enzyme. PKM2 might, on the other hand, function as a protein kinase, which usually occurs after PKM2 nuclear translocation and is a direct consequence of its detetramerization. PKM2 has been shown to participate in regulating gene transcription [18,19] and controlling the functions and activation of immune cells such as dendritic cells and macrophages [13,36,37], which may be attributable in part to the fact that PKM2 nuclear translocation regulates Hif-1 activity and interleukin-1 (IL-1) induction [38]. In addition, PKM2 nuclear translocation can also promote tumor angiogenesis by regulating hypoxia-inducible Factor-1α (HIF-1α) through nuclear factor-kappa B (NF-κB) activation [39]. Consistent with these findings, our study found that the nuclear translocation of PKM2 contributes to the activation of glial cells in ICH, possibly by functioning as a protein kinase. However, the specific mechanisms underlying this process have not been thoroughly investigated. Even though we did not investigate the metabolic enzyme role of PKM2 in regulating glial activation and brain injury of ICH, we speculate that the enzymatic activity of PKM2 may also contribute to glial activation and brain injury after ICH, because 70% of PKM2+ glial cells lacked obvious nuclear translocation, although their exact roles in the brain injury of ICH require further investigation. This may also explain why TEPP-46 treatment only enhanced the motor function recovery of mice with ICH, but not the sensory function recovery, as the TEPP-46 treatment only inhibited the PKM2 nuclear translocation without affecting its total expression. Therefore, we hypothesize that the function of PKM2 involved in the ICH-induced pathological changes may be related to the enhancement of glycolytic rate to produce more ATP and the promotion of glial cell gene expression, both of which promote the activation of glial cells after ICH.

Furthermore, comprehending the glial activation upon ICH requires a knowledge of the mechanism triggering the PKM2 tetramer to monomer transition. One previous study found that the upregulation of astrocytic signal transducer and activator of transcription 3 (STAT3) signaling was related to nuclear translocation of PKM2 [40] and, combined with our and others' findings, indicates that STAT3 signaling is increased in response to brain damage induced by ICH [23,41]. Accordingly, we hypothesize that the increased STAT3 signaling may contribute to PKM2 detetramerization in glial cells after ICH.

Furthermore, we performed RNA-seq to investigate the potential mechanisms of inhibition of PKM2 nuclear translocation on influencing the brain injury of ICH. We found that more than 90% of DEGs were down-regulated in ICH mice treated by TEPP-46, indicating that inhibition of PKM2 nuclear translocation may reverse the highly expressed genes triggered by ICH. As TEPP-46 treatment could both decrease glial activation and reduce the brain damage of ICH, we performed a conjoint analysis of the down-regulated DEGs of perihematomal brain tissues with previously published transcriptome data of neural cells to investigate potential changes in neural cells after ICH in mice treated with or without TEPP-46. The majority of down-regulated DEGs were found in neurons, followed by microglia, endothelial cells, and astrocytes. Notably, 15.58% (12/77) of down-regulated DEGs were specifically highly expressed in neurons, further suggesting that these genes may be involved in the regulation of neuronal activity, injury, and death after ICH, either directly or indirectly influenced by the glial activation caused by TEPP-46 treatment.

Nevertheless, our study has some limitations. For instance, even though we found that TEPP-46 treatment offers neuroprotective benefits for ICH mice, given that PKM2 is extensively expressed in numerous cells and organs, it remains to be determined whether and to what extent it influences the function of peripheral organs. In addition, the specificity of TEPP-46 on stabilizing PKM2 tetramer formation in ICH brains remains to be thoroughly evaluated. Therefore, despite that we might have discovered a potential therapeutic treatment for ICH, these limitations will impact whether TEPP-46 can be applied clinically. As a result, considerably more effort is required to translate our results into effective therapy.

5. Conclusions

This study investigated the protein kinase activity of PKM2 in the regulation of glial activation and brain damage caused by ICH. The increased PKM2 nuclear translocation that we have shown provides new molecular insights into glial activation during ICH pathogenesis and offers a potential therapeutic strategy for reducing ICH-induced brain damage.

Availability of Data and Materials

The datasets of this study are available from the corresponding authors upon request. The datasets of RNA-seq for this study can be found in the GEO accession GSE205082.

Author Contributions

Conceptualization: YT, SGY and XYX; Investigation/Methodology: YJL, XXZ, SHY, ZQZ, SQL, and JYS; Writing - original draft: XYX; Writing - review & editing: SGY. All authors contributed to editorial changes in the manuscript. All authors read and approved the final manuscript. All authors have participated sufficiently in the work and agreed to be accountable for all aspects of the work.

Ethics Approval and Consent to Participate

The animal study was reviewed and approved by Animal Ethics Committee of Chengdu University of Traditional Chinese Medicine (CDUTCM-2020-0116).

Acknowledgment

Not applicable.

Funding

This work was supported by the Science Foundation for Distinguished Young Scholars of the Science and Technology Department of Sichuan Province (2020JDJQ0046).

Conflict of Interest

The authors declare no conflict of interest.

References

[1] Hemphill JC, 3rd, Greenberg SM, Anderson CS, Becker K, Bendok BR, Cushman M, *et al*. Guidelines for the Management of Spontaneous Intracerebral Hemorrhage: A Guideline for Healthcare Professionals From the American Heart Association/American Stroke Association. Stroke. 2015; 46: 2032–2060.

[2] Macellari F, Paciaroni M, Agnelli G, Caso V. Neuroimaging in intracerebral hemorrhage. Stroke. 2014; 45: 903–908.

[3] Xiong XY, Liu L, Yang QW. Functions and mechanisms of microglia/macrophages in neuroinflammation and neurogenesis after stroke. Progress in Neurobiology. 2016; 142: 23–44.

[4] Zhou Y, Wang Y, Wang J, Anne Stetler R, Yang QW. Inflammation in intracerebral hemorrhage: from mechanisms to clinical translation. Progress in Neurobiology. 2014; 115: 25–44.

[5] Amor S, Puentes F, Baker D, van der Valk P. Inflammation in neurodegenerative diseases. Immunology. 2010; 129: 154–169.

[6] Supplie LM, Düking T, Campbell G, Diaz F, Moraes CT, Götz M, *et al*. Respiration-Deficient Astrocytes Survive As Glycolytic Cells *In Vivo*. The Journal of Neuroscience: the Official Journal of the Society for Neuroscience. 2017; 37: 4231–4242.

[7] Goyal MS, Hawrylycz M, Miller JA, Snyder AZ, Raichle ME. Aerobic glycolysis in the human brain is associated with development and neotenous gene expression. Cell Metabolism. 2014; 19: 49–57.

[8] Dienel GA, Cruz NF. Aerobic glycolysis during brain activation: adrenergic regulation and influence of norepinephrine on astrocytic metabolism. Journal of Neurochemistry. 2016; 138: 14–52.

[9] Israelsen WJ, Dayton TL, Davidson SM, Fiske BP, Hosios AM, Bellinger G, *et al*. PKM2 isoform-specific deletion reveals a differential requirement for pyruvate kinase in tumor cells. Cell. 2013; 155: 397–409.

[10] Luo W, Semenza GL. Emerging roles of PKM2 in cell metabolism and cancer progression. Trends in Endocrinology and Metabolism: TEM. 2012; 23: 560–566.

[11] Mazurek S, Boschek CB, Hugo F, Eigenbrodt E. Pyruvate kinase type M2 and its role in tumor growth and spreading. Seminars in Cancer Biology. 2005; 15: 300–308.

[12] Yang L, Xie M, Yang M, Yu Y, Zhu S, Hou W, *et al*. PKM2 regulates the Warburg effect and promotes HMGB1 release in sepsis. Nature Communications. 2014; 5: 4436.

[13] Jin X, Zhang W, Wang Y, Liu J, Hao F, Li Y, *et al*. Pyruvate Kinase M2 Promotes the Activation of Dendritic Cells by Enhancing IL-12p35 Expression. Cell Reports. 2020; 31: 107690.

[14] Pan RY, He L, Zhang J, Liu X, Liao Y, Gao J, *et al*. Positive feedback regulation of microglial glucose metabolism by histone H4 lysine 12 lactylation in Alzheimer's disease. Cell Metabolism. 2022; 34: 634–648.e6.

[15] Dayton TL, Jacks T, Vander Heiden MG. PKM2, cancer metabolism, and the road ahead. EMBO Reports. 2016; 17: 1721–1730.

[16] Palsson-McDermott EM, O'Neill LAJ. The Warburg effect then and now: from cancer to inflammatory diseases. BioEssays: News and Reviews in Molecular, Cellular and Developmental Biology. 2013; 35: 965–973.

[17] Wong N, Ojo D, Yan J, Tang D. PKM2 contributes to cancer metabolism. Cancer Letters. 2015; 356: 184–191.

[18] Yang W, Lu Z. Pyruvate kinase M2 at a glance. Journal of Cell Science. 2015; 128: 1655–1660.

[19] Hsu MC, Hung WC. Pyruvate kinase M2 fuels multiple aspects of cancer cells: from cellular metabolism, transcriptional regulation to extracellular signaling. Molecular Cancer. 2018; 17: 35.

[20] Xiong XY, Tang Y, Yang QW. Metabolic changes favor the activity and heterogeneity of reactive astrocytes. Trends in Endocrinology and Metabolism: TEM. 2022; 33: 390–400.

[21] Liang YJ, Yang YR, Tao CY, Yang SH, Zhang XX, Yuan J, *et al*. Deep Succinylproteomics of Brain Tissues from Intracerebral Hemorrhage with Inhibition of Toll-Like Receptor 4 Signaling. Cellular and Molecular Neurobiology. 2022; 42: 2791–2804.

[22] Deng YH, Zhang XX, Tao CY, Liang YJ, Yuan J, Yang SH, *et al*. Succinylation profiles of brain injury after intracerebral hemorrhage. PloS One. 2021; 16: e0259798.

[23] Xiong XY, Liu L, Wang FX, Yang YR, Hao JW, Wang PF, *et al*. Toll-Like Receptor 4/MyD88-Mediated Signaling of Hepcidin Expression Causing Brain Iron Accumulation, Oxidative Injury, and Cognitive Impairment After Intracerebral Hemorrhage. Circulation. 2016; 134: 1025–1038.

[24] Alim I, Caulfield JT, Chen Y, Swarup V, Geschwind DH, Ivanova E, *et al*. Selenium Drives a Transcriptional Adaptive Program to Block Ferroptosis and Treat Stroke. Cell. 2019; 177: 1262–1279.e25.

[25] Karuppagounder SS, Alim I, Khim SJ, Bourassa MW, Sleiman SF, John R, *et al*. Therapeutic targeting of oxygen-sensing prolyl hydroxylases abrogates ATF4-dependent neuronal death and improves outcomes after brain hemorrhage in several rodent models. Science Translational Medicine. 2016; 8: 328ra29.

[26] Li H. Minimap2: pairwise alignment for nucleotide sequences. Bioinformatics (Oxford, England). 2018; 34: 3094–3100.

[27] Zhou X, Lindsay H, Robinson MD. Robustly detecting differential expression in RNA sequencing data using observation weights. Nucleic Acids Research. 2014; 42: e91.

[28] UniProt Consortium. Activities at the Universal Protein Resource (UniProt). Nucleic Acids Research. 2014; 42: D191–D198.

[29] Zhang Y, Chen K, Sloan SA, Bennett ML, Scholze AR, O'Keeffe S, *et al*. An RNA-sequencing transcriptome and splicing database of glia, neurons, and vascular cells of the cerebral

cortex. The Journal of Neuroscience: the Official Journal of the Society for Neuroscience. 2014; 34: 11929–11947.

[30] Zhang J, Feng G, Bao G, Xu G, Sun Y, Li W, *et al*. Nuclear translocation of PKM2 modulates astrocyte proliferation via p27 and -catenin pathway after spinal cord injury. Cell Cycle (Georgetown, Tex.). 2015; 14: 2609–2618.

[31] Anastasiou D, Yu Y, Israelsen WJ, Jiang JK, Boxer MB, Hong BS, *et al*. Pyruvate kinase M2 activators promote tetramer formation and suppress tumorigenesis. Nature Chemical Biology. 2012; 8: 839–847.

[32] Spoden GA, Mazurek S, Morandell D, Bacher N, Ausserlechner MJ, Jansen-Dürr P, *et al*. Isotype-specific inhibitors of the glycolytic key regulator pyruvate kinase subtype M2 moderately decelerate tumor cell proliferation. International Journal of Cancer. 2008; 123: 312–321.

[33] Spoden GA, Rostek U, Lechner S, Mitterberger M, Mazurek S, Zwerschke W. Pyruvate kinase isoenzyme M2 is a glycolytic sensor differentially regulating cell proliferation, cell size and apoptotic cell death dependent on glucose supply. Experimental Cell Research. 2009; 315: 2765–2774.

[34] Christofk HR, Vander Heiden MG, Harris MH, Ramanathan A, Gerszten RE, Wei R, *et al*. The M2 splice isoform of pyruvate kinase is important for cancer metabolism and tumour growth. Nature. 2008; 452: 230–233.

[35] Xie M, Yu Y, Kang R, Zhu S, Yang L, Zeng L, *et al*. PKM2-dependent glycolysis promotes NLRP3 and AIM2 inflammasome activation. Nature Communications. 2016; 7: 13280.

[36] Liu C, Zheng M, Wang T, Jiang H, Fu R, Wang H, *et al*. PKM2 Is Required to Activate Myeloid Dendritic Cells from Patients with Severe Aplastic Anemia. Oxidative Medicine and Cellular Longevity. 2018; 2018: 1364165.

[37] Zhang Z, Liu Q, Che Y, Yuan X, Dai L, Zeng B, *et al*. Antigen presentation by dendritic cells in tumors is disrupted by altered metabolism that involves pyruvate kinase M2 and its interaction with SOCS3. Cancer Research. 2010; 70: 89–98.

[38] Palsson-McDermott EM, Curtis AM, Goel G, Lauterbach MAR, Sheedy FJ, Gleeson LE, *et al*. Pyruvate kinase M2 regulates Hif-1α activity and IL-1β induction and is a critical determinant of the warburg effect in LPS-activated macrophages. Cell Metabolism. 2015; 21: 65–80.

[39] Azoitei N, Becher A, Steinestel K, Rouhi A, Diepold K, Genze F, *et al*. PKM2 promotes tumor angiogenesis by regulating HIF-1α through NF-κB activation. Molecular Cancer. 2016; 15: 3.

[40] Borbor M, Yin D, Brockmeier U, Wang C, Doeckel M, Pillath-Eilers M, *et al*. Neurotoxicity of ischemic astrocytes involves STAT3-mediated metabolic switching and depends on glycogen usage. Glia. 2023; 71: 1553–1569.

[41] Liang Z, Wu G, Fan C, Xu J, Jiang S, Yan X, *et al*. The emerging role of signal transducer and activator of transcription 3 in cerebral ischemic and hemorrhagic stroke. Progress in Neurobiology. 2016; 137: 1–16.